

THE INS 176cm SECTOR FOCUSING CYCLOTRON

Y. Hirao, T. Tanabe, M. Sekiguchi, K. Sato, M. Fujita, T. Yamazaki, Y. Sakurada, T. Honma, N. Yamazaki, M. Furuya, T. Yamada\* and H. Ogawa\*

Institute for Nuclear Study, University of Tokyo, 3-2-1 Midori-cho, Tanashi, Tokyo, Japan

\*Present address: National Institute of Radiological Sciences, Chiba, Japan

Abstract

Construction of the INS 176cm Sector Focusing Cyclotron was completed and the first extracted beam was got about one year ago.

Energy ranges are as follows :  $E_p=7.5 \sim 48$ ,  $E_d=15 \sim 34$ ,  $E_H=23 \sim 90$ ,  $E_\alpha=30 \sim 68$ , and  $E=68 \text{ g}^2/\text{A MeV}$ .

Design study, mechanical structure, measurement of magnetic field, and measurement of inner and extracted beams using three types of beam probes are reported. The RF system consists of self oscillator, booster and dee voltage stabilizer.

For polarized ion, an axial injection system is installed.

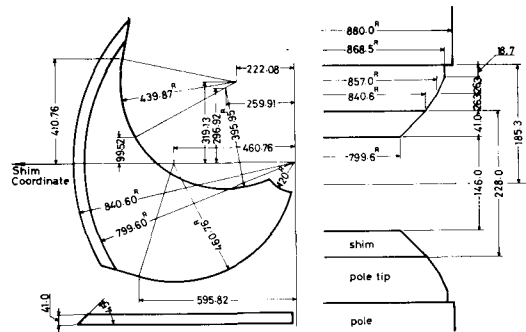


Fig.2 Pole profile and spiral shim of the magnet

1. Magnet

Before constructing the magnet, a 1/8.8 scale model was tested. Detailed studies on orbit analysis, extraction analysis and central region magnetic field were performed using a 1/1.6 scale model. On the basis of these data and analyses, the magnet and spiral shims was manufactured as shown in Figs. 1 and 2.

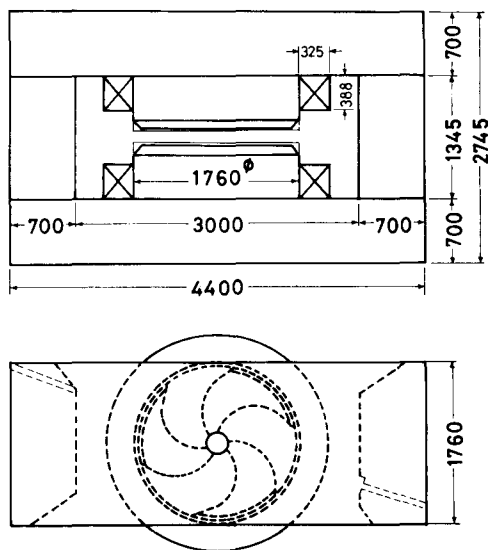


Fig. 1 Dimensions of the magnet

The tolerances for the six sectors being identical, for the setting of 120° symmetry around the magnet center, and for the homogeneities of hill and valley gap widths, are kept within ±0.025mm, ±7" and ±0.005 mm, respectively. Magnetic field in the median plane was measured within an accuracy of 1 gauss using a Siemens FC-33 Hallgenerator rotated azimuthally in the median plane at 4° intervals with a tolerance of ±15". In order to test the adequacy of the tolerances for machining and installation, the amplitude of the first harmonic component of the magnetic field was observed. From the analysis of radial stability, the maximum tolerable first harmonic should be a few gauss. The measured result shows that the amplitude is sufficiently well suppressed as to maintain radial stability for every particle.

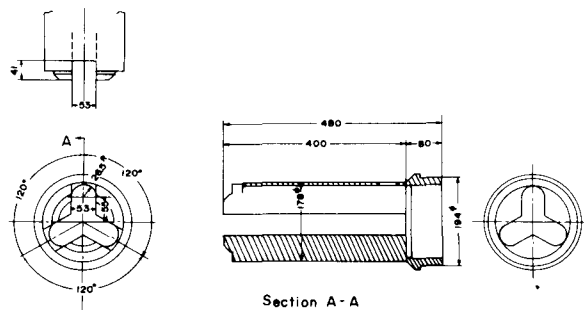


Fig. 3 Center plug

The shape of center plug was decided as shown in Fig.3 after several model tests using the 1/1.6 scale model magnet. The plugs have driving mechanism of two degrees of freedom ( $\theta$  and  $z$ ), as shown in Fig. 9. An important roll of center plug is to form an appropriate field bump in the center region by adjusting axial position, as shown in Figs.5 and 6.

The effect of the circular trim coils are shown in Fig. 4. These coils consist of 11 sets of pole face windings of mineral-insulated cable.

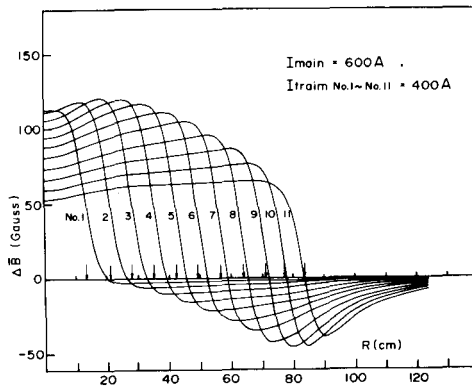


Fig. 4 Radial dependence of the effects of circular trim coils. Arrow indicates the position of each trim coil.

We obtained detailed information concerning the orbit properties by numerical intergration of the differential equations representing the particle orbit. First, the isochronous field was calculated. Then the optimum currents of the main coil and eight trimming coils were determined so as to fit the isochronous field by the least squares method. Axial and radial betatron frequencies were calculated for the field corrected by trimming coils. Figs. 5 and 6 show the results for the maximum energy of H<sup>+</sup> and He<sup>++</sup> ions, respectively. The field deviations from isochronous fields are generally less than ±5 Gauss.

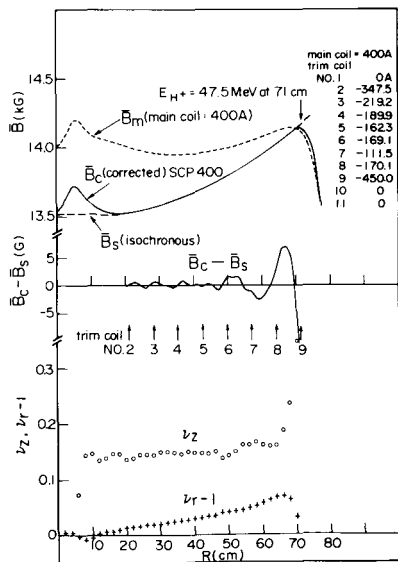


Fig. 5 Corrected field using eight pairs of trimming coils, field deviation from the isochronous field, and betatron frequencies

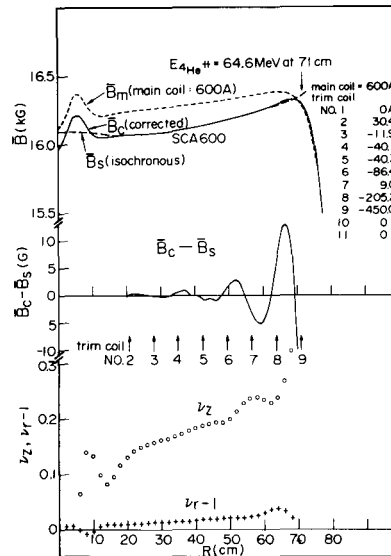


Fig.6 The same as Fig. 5

Magnetic field along the axis through the center hole of the magnet was measured. Fig. 7 show the results for several levels of field excitation. The curves exhibit a very rapid field increasing at a distance between 7 and 20 cm from the center of the magnet.

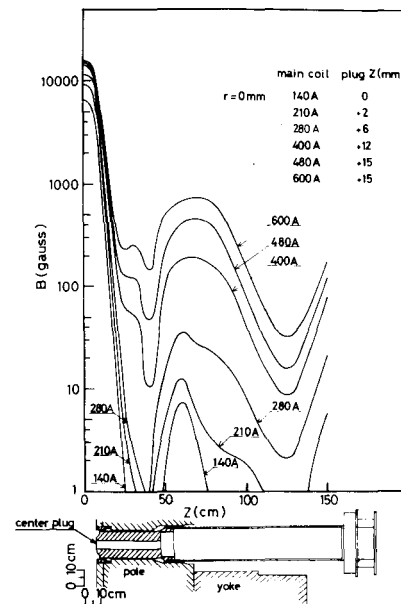


Fig. 7 Magnetic field along the axis of the center hole of the magnet

### 2. RF system

A booster and self-oscillator system, as shown in Fig. 8 was adopted. The useful frequency range of the oscillator system covers the range, 7.5-22.5 MHz. The mechanisms for varying resonance frequency (movable short) and adjusting input impedance (movable coupling capacitor) are also functioning well.

Frequency stability is higher than  $10^{-4}$  without stabilizer and  $10^{-5}$  with stabilizer using two small compensating capacitors and crossing counter circuit as a feedback loop. A low  $\mu$  power triode (ITT-F-6379) is connected in series to the power supply and is used as a unit of the dee voltage stabilizer. Using this system, drift of the dee voltage is  $2.5 \times 10^{-4}/30$  min.

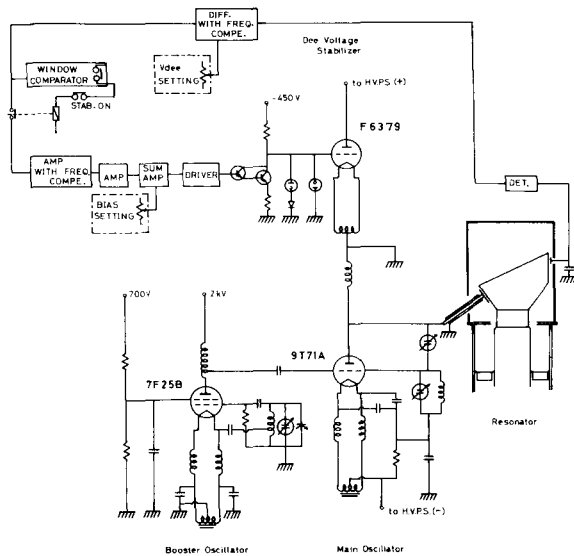


Fig. 8 Circuit diagram of the booster, self-oscillator and dee voltage stabilizer system

### 3. Ion source

A normal type of ion source is inserted axially from bottom of the magnet. Structure of the ion source is a normal water-cooled hot cathode type. It has a moving mechanism of four degrees of freedom ( $r, \theta, z$  and rotation). The puller also has a moving mechanism of three degrees of freedom ( $r, \theta$ , and rotation).

Polarized  $H^+$  and  $D^+$ , and some heavy ions, which are difficult to make with inner ion source, are planned to be injected axially through the upper hole of the magnet. In the case of axial injection an electrostatic mirror is inserted axially from bottom of the magnet in place of the normal inner ion source.

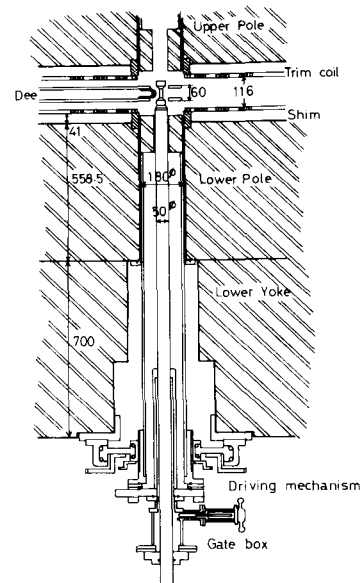


Fig. 9 Driving mechanism of central plug and ion source

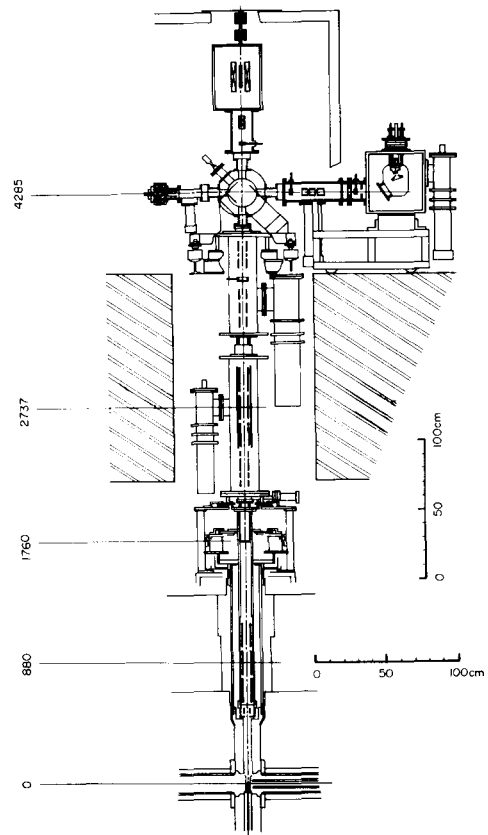


Fig. 10 Beam injection system from the upper side of the main magnet

4. Beam extraction system

The beam extraction system consists of two electrostatic deflectors. Parallel plate and quadrupole type electrodes were chosen for the first and second deflectors, respectively, whose maximum strength of electric field is assumed to be 100 KV/cm. Entrance of the first deflector is located near the center of the hill in the azimuthal direction and at a radius of 74.5 cm.

5. Beam probe

As shown in Fig.11, three probes are available at the same time. They can move along three radial directions at the angles of 5° (Dee Probe), 132° (Deflector Probe) and 226.5° (Main Probe) with respect to the RF resonator axis. For the Main Probe, differential, three finger and phase probes are prepared.

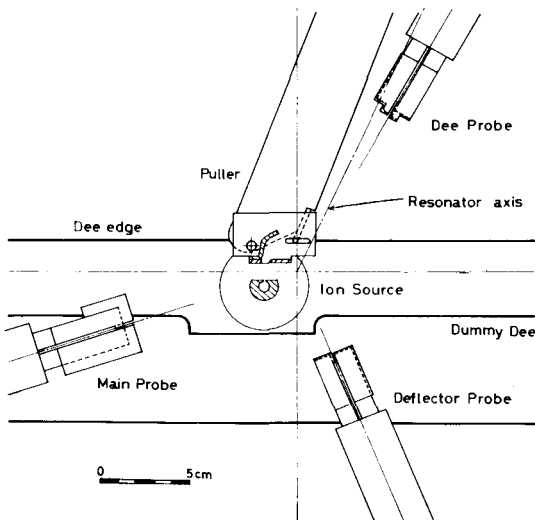


Fig. 11 Layout of the central region

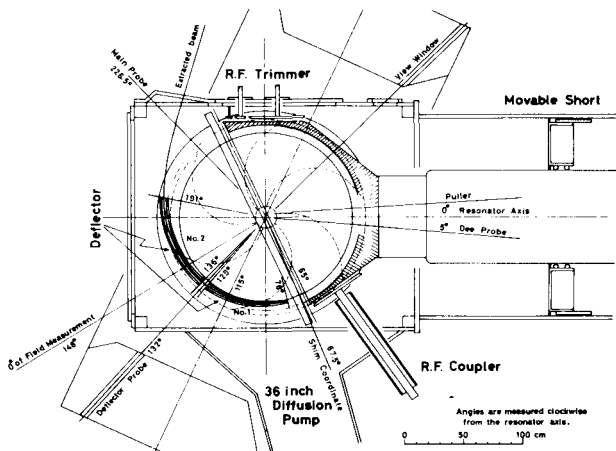


Fig. 12 Lay-out in vacuum chamber

The lay-out around the vacuum chamber is shown in Fig. 13. This lay-out was decided as the most suitable for the beam extraction. The relative position of the spiral shims in the figure is shown by the "shim coordinate" designated in Figs. 2 and 12.

6. Beam acceleration

Two kinds of ions were accelerated to full radius at several magnetic field excitations. The energies were 7.5, 9, 10, 14 and 28 MeV for  $H^+$  and 67 MeV for  ${}^4He^{++}$ . Sometimes test was performed using  $H_2^+$  ion to simulate  $D^+$  and  ${}^4He^{++}$  acceleration. A typical turn pattern observed by using the differential beam probe (Deflector Probe) is shown in Fig. 13.

Beam phase was observed by the frequency and field detuning method or using the phase probe. For the isochronous field, measured phases were within  $1^\circ$  and are in good agreement with calculation.

7. Beam extraction

Beam extraction test was performed for  ${}^4He^{++}$  of 67 MeV and  $H^+$  of 10 MeV which correspond to maximum and nearly minimum magnetic fields, respectively. These beams were extracted to the direction expected from the magnetic field measurements and the floating wire measurements, by adjusting the voltages and the positions of the deflectors. Extraction efficiencies for the inner beam at the maximum radius were 80 % and 70 % at the exits of the first and second deflectors, respectively.

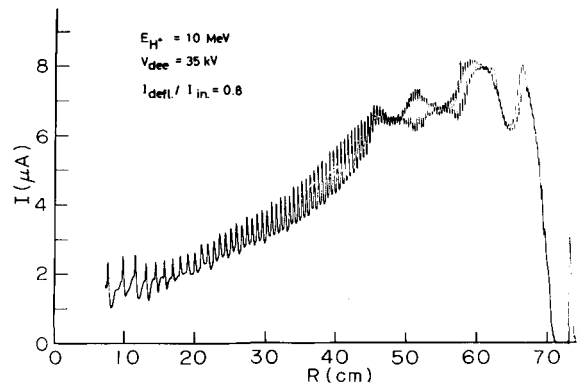


Fig. 13 A typical turn pattern observed by the differential probe